

Gold Layers on Elastomers near the Critical Stress Regime

Bekim Osmani, Hans Deyhle, Tino Töpfer, Thomas Pfohl, and Bert Müller*

Soft electrodes are essential components of soft robotics, tunable optics, microfluidics, flexible electronics, neuroprosthetics, and dielectric elastomeric transducers (DET). The two main paths employed to increase an electrode's compliance involve the manipulation of either its intrinsic material properties or its structural features, such as the introduction of wrinkles, which arise above the critical stress of metal films on elastomeric substrates. Herein, this study demonstrates that the interplay between functionalized oxygen-plasma-treated polydimethylsiloxane (PDMS) films and sputter-deposited metal electrodes allows for conserving compressive stress within the electrode. Insulator–metal transition already occurs for 10 nm thin Au electrodes, and below this electrode thickness, atomic force microscopy nanoindentations with sub-micrometer resolutions reveal no stiffening of the Au/PDMS heterostructure. These DETs exhibit reduced electrocreasing, which is a significant contributor to structural failure, while their enhanced dielectric breakdown field of up to $120 \text{ V } \mu\text{m}^{-1}$ enables calculated strains above 10% — a crucial requirement for thin-film DETs such as those used for artificial muscles.

1. Introduction

Recently, dielectric elastomer transducers (DET), also known as artificial muscles, have attracted broad interest, due to their versatile applicability as dielectric elastomer actuators (DEA), sensors, self-sensing actuators, and electric generators.^[1–5] They are essential building blocks for applications in medicine, soft robotics, microfluidics, and flexible optoelectronics.^[4,6–8] Very recently, Poulin et al. presented a fully printed $3 \mu\text{m}$ thin DEA, in which the operating voltage could be reduced from the kilovolt range to some hundreds of volts.^[9] For future medical implants, however, nanometer-thin DEAs are required, as they can operate at physiologically acceptable voltages below 12 V.^[10,11] Generally, planar DEAs are sandwich structures in which, for example, polydimethylsiloxane (PDMS) as an elastomeric film is embedded between soft electrodes and transduces electrical energy into mechanical work, as electrostatic pressure drives the elastomer to expand laterally by tens of percent.^[12,13] A major goal is the development of nanometer-thin flexible and

stretchable electrodes for a few micrometer- or sub-micrometer-thin DEAs. Many materials and related fabrication and characterization methods have been proposed for electrodes, including carbon powder, metallic thin films, or the implantation of metal nanoclusters.^[14–18] Another approach to stretchable electronics, presented by Hirsch et al., is based on biphasic AuGa_2/Ga solid–liquid thin metal films. However, rigid 60 nm sputtered Au metallization is still required,^[19] which significantly stiffens the overall thin-film DEA.^[9,20] A related challenge is the low adhesion of Au to PDMS,^[21] which can be improved via Cr or Ti layers but also increases the overall stiffness.^[22] Atmaja et al. have shown that (3-mercaptopropyl)trimethoxysilane (MPTMS) can be used as a molecular adhesive to transfer atomically flat Au films to PDMS surfaces.^[23] In addition, Mahapatro et al.

have demonstrated that deposited Au on a self-assembled monolayer of MPTMS on an oxidized Si substrate has a root-mean-square surface roughness in the sub-nanometer scale.^[24] MPTMS is a bifunctional molecule, its thiol head ($-\text{SH}$) binds to Au and the three methoxy ($-\text{OCH}_3$) functional groups bind to hydroxy PDMS ($-\text{OH}$) surfaces, which can be introduced by oxygen plasma or ultraviolet/ozone treatments.^[20] Oxygen plasma forms a silica-like film on top of the PDMS layer,^[25–27] thereby leading to a wrinkled surface, as its thermal expansion coefficient is several orders of magnitude lower compared to that of the underlying bulk PDMS.^[28] Wrinkling is a universal phenomenon exhibited by a compressed film resting on a flexible substrate. Many approaches have been presented to control and even delaminate buckling films for enhanced stretchability.^[29,30] As reported by Bowden et al., compressive stress in the SiO_x film has to exceed a critical stress for wrinkles to arise.^[31,32] The critical stress can be described as a function of the elastic moduli of the upper film and the elastomer bulk.^[33] Hendricks and Lee showed that by incorporating nanoparticles into the film, they were able to control and even prevent polymer films from buckling.^[34] Herein, we illustrate that by depositing Au on MPTMS-functionalized and oxygen-plasma-treated PDMS (PDMS-O_x) films near the critical stress regime, we can conserve compressive stress and fabricate flat or wrinkled Au electrodes with a negligible stiffness increase in the overall Au/PDMS heterostructure. Using this technique, we have fabricated DEAs on polyethylene naphthalate (PEN) substrates and quantified actuation by using an in-house-built optical beam deflection device with applicable electrical fields up to $120 \text{ V } \mu\text{m}^{-1}$.^[35]

B. Osmani, Dr. H. Deyhle, Dr. T. Töpfer, Dr. T. Pfohl, Prof. B. Müller
Biomaterials Science Center
Department of Biomedical Engineering
University of Basel
Allschwil 4123, Switzerland
E-mail: bert.mueller@unibas.ch

 The ORCID identification number(s) for the author(s) of this article can be found under <https://doi.org/10.1002/admt.201700105>.

DOI: 10.1002/admt.201700105

1.1. Fabrication of Compressed Au Electrodes on a Wrinkled PDMS Film

The wrinkling and buckling phenomena of films on elastomeric substrates are well understood.^[32,33,36] Compressive or buckling stress σ_{comp} can be generated mechanically or thermally, as outlined in Equation (1)

$$\sigma_{\text{comp}} = \frac{E_f (\alpha_s - \alpha_f) (T_{\text{dep}} - T_{\text{room}})}{64 (1 - \nu_f^2)} \quad (1)$$

The thermal expansion coefficient of the bulk PDMS α_s is usually several orders of magnitude larger than that of a metallic or a silica-like film α_f . The deposition of the metallic film as well as the plasma treatment of the PDMS substrate takes place at an elevated temperature T_{dep} , so the film may undergo buckling as the structure cools down to T_{room} in order to release compressive stress. It is reported that the film only wrinkles if the compressive stress is greater than a critical stress σ_{crit} , which is described as a function of the elastic moduli $E_{s,f}$ and the Poisson's ratios $\nu_{s,f}$ of the substrate and the film,^[31,33] respectively

$$\sigma_{\text{crit}} = \left(\frac{9E_f E_s^2}{64(1-\nu_f^2)(1-\nu_s^2)^2} \right)^{1/3} \quad (2)$$

The orientation of the wrinkles on bulk PDMS is generally random, but the periodicity λ is reported to be proportional to the metal- or silica-like film height h_f ^[30–32]

$$\lambda = 2\pi h_f \left(\frac{(1-\nu_f^2)E_f}{3(1-\nu_s^2)E_s} \right)^{1/3} \quad (3)$$

Similar to the deposition of metallic films, during oxygen-plasma treatment, the PDMS surface is heated while a stiff, silica-like layer is formed.^[26,32] During cooling, stress is released by forming wrinkle-like structures on top of the elastomer layer. The thickness of the silica-like layer is estimated on the basis of the buckling model for a bilayer system. Applying Equation (3) to selected PDMS films with Young's moduli of (1.0 ± 0.1) and (0.2 ± 0.1) MPa, the periodicities of the wrinkle patterns correspond to 2.6 and 4.5 μm , respectively. Assuming an elastic modulus for the silica-like layer of 1.5 GPa, as suggested by B efahy et al.,^[37] one finds a layer thickness of about 50 nm. Transmission electron microscopy (TEM) images of B efahy et al.^[37] show that the thickness of the silica-like layer can be controlled adjusting the plasma power and treatment time.

We show in **Figure 1A** the reformation of a thermally cured, plasma-treated PDMS layer (PDMS- O_x) with prominent wrinkles. The periodicity of the wrinkles was found to be $\lambda = (2.0 \pm 0.1)$ μm , using a 2D Fast Fourier Transform (2D FFT) analysis of the related atomic force microscopy (AFM) image. No preferential orientation of the wrinkles could be observed. The evaporation of a 30 nm thin Au electrode inside an ultra-high vacuum (UHV) chamber from a 45 cm-distant effusion source did not alter the periodicity or amplitude of the wrinkled pattern (Figure 1B). However, the sputtering of 30 nm thin Au

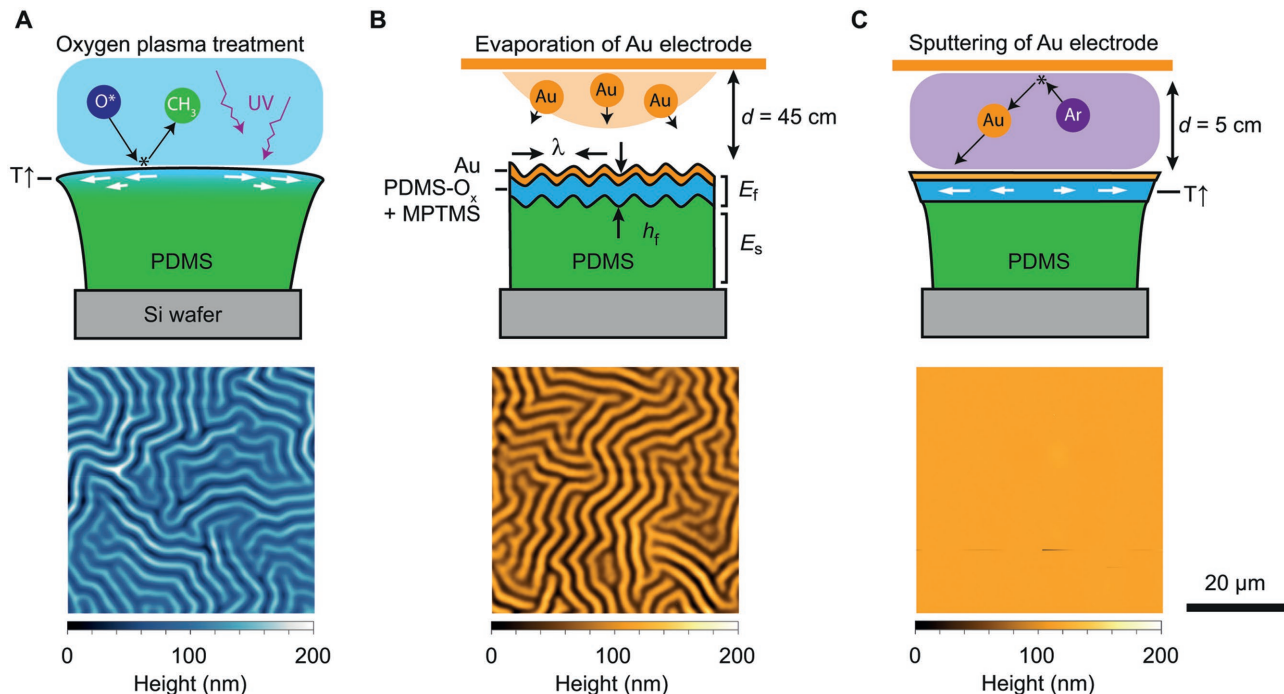


Figure 1. Fabrication of compressed Au electrodes on PDMS substrates. A) Schematic representation of PDMS surface modifications, using oxygen-plasma treatment (400 W, 120 s, 20 sccm oxygen flow). An AFM scan of a $50 \times 50 \mu\text{m}^2$ region after the oxygen-plasma treatment. The changed topography is due to induced stress in the silica-like layer on top of the PDMS layer. The characteristic wrinkles were prominent features with a periodicity of 2 μm and the amplitude of 90 nm. B) Thermal evaporation of 30 nm thin Au at a distance of 45 cm in UHV did not alter the wrinkled structure. C) Schematic representation of the sputtering process and AFM scan of a $50 \times 50 \mu\text{m}^2$ region after the sputtering of 30 nm thin Au, where the very top of the PDMS film is reheated and flattened during the sputter deposition of the Au electrode.

on the same substrate from a 5 cm-distant Au target flattened the surface completely (Figure 1C).

1.2. From Wrinkled to Flat Compressed Au/PDMS Heterostructures

We show in Figure 2 that there is no abrupt change from wrinkling to nonwrinkling near the critical stress regime. The wrinkle amplitudes from the height histograms of the AFM scans were found to be (61 ± 3) nm for the oxygen plasma-treated

PDMS. No preferential orientation of the wrinkles could be observed. After the subsequent sputtering of 5 nm Au, the wrinkles were maintained, cf. Figure 2B. 2D FFT analysis showed a slightly reduced periodicity of $\lambda = (1.9 \pm 0.1)$ μm , while the amplitude of the wrinkles was reduced to (33 ± 2) nm. For a 7 nm thin Au electrode, as shown in Figure 2C, the wrinkles almost disappeared. A cross-section revealed very flat wrinkles with an average height of (3 ± 1) nm and a periodicity of $\lambda = (2.3 \pm 0.1)$ μm . The mapping of the mechanical properties of the oxygen plasma-treated PDMS and Au/PDMS heterostructures revealed anisotropy on the sub-micrometer scale.

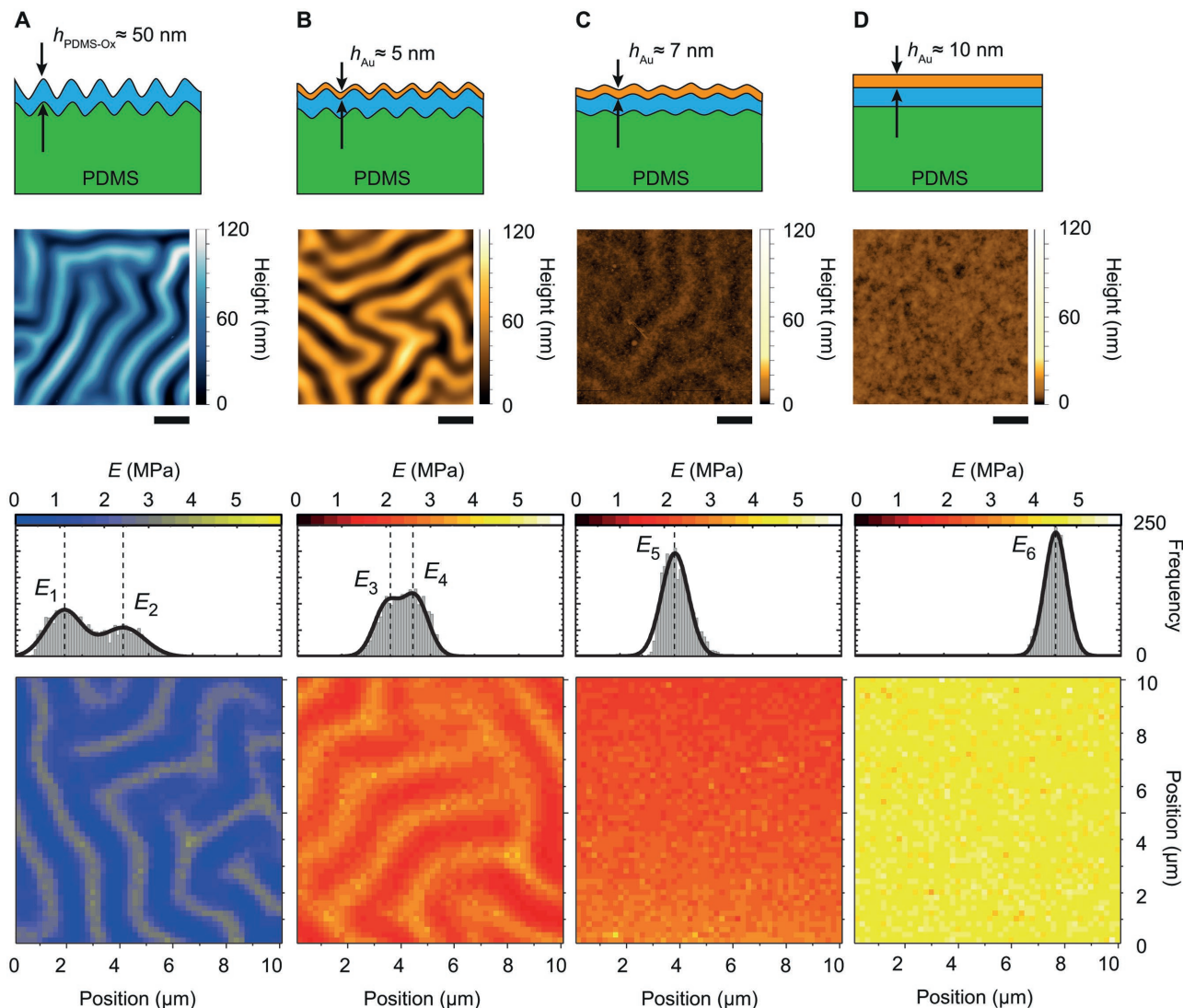


Figure 2. Evolution of oxygen-plasma-induced wrinkles toward compressed Au electrodes. A) Schematic of the oxygen-plasma-treated PDMS. The periodicity of the wrinkles was found to be (2.0 ± 0.1) μm with the average amplitude of (61 ± 3) nm as extracted from the AFM scan shown below. The bar corresponds to 2 μm . A stiffness histogram extracted from 2500 nanoindentations shows one peak at $E_1 = (1.1 \pm 0.5)$ MPa and a second peak at $E_2 = (2.4 \pm 0.5)$ MPa. The stiffness map with a sub-micrometer resolution identifies that the two peaks found in the histogram correspond to the softer material in valleys rather than on the hills. B) After the subsequent sputtering of 5 nm Au, the wrinkles were maintained with a slightly reduced periodicity of (1.9 ± 0.1) μm . The amplitude was reduced to (33 ± 2) nm. The related stiffness histogram shows a peak at $E_3 = (2.1 \pm 0.3)$ MPa and at $E_4 = (2.7 \pm 0.3)$ MPa. C) For a 7 nm Au electrode, the wrinkles were hardly recognized. The amplitude could not be extracted from the height histogram. Stiffness histograms show only one peak at $E_5 = (2.2 \pm 0.4)$ MPa. D) A deposition of 10 nm thin Au flattened the surface completely. Its mean surface roughness value of about 1 nm was similar to sputtered 10 nm thin Au on native PDMS. The related stiffness histogram shows only one peak at $E_6 = (4.5 \pm 0.3)$ MPa.

Probing of the wrinkled film with the AFM tip for each 200 nm shows that material in valleys is softer than that on hills. For the given plasma treatment parameters (RF power 200 W, treatment duration 120 s, oxygen pressure 0.3 mbar), valleys show an average elastic modulus of $E_1 = (1.1 \pm 0.5)$ MPa compared to hills with an elastic modulus of $E_2 = (2.4 \pm 0.5)$ MPa. The topological information required to discriminate between valleys and hills was extracted from the quasi height nanoindentation map. One can only speculate on the nature of the measured micrometer-scale modulations of the elastic modulus. Besides geometrical phenomena, the thickness modulation of the silica-like layer, possibly induced by the material transport,^[38] is a plausible explanation. The nanoindentation depths were maximal 200 nm at a silica-like layer thickness of about 50 nm. The related histograms in Figure 2 show that after the sputter deposition of Au, compressive stress suppressed the stiffening effect, with $E_3 = (2.1 \pm 0.3)$ MPa, $E_4 = (2.7 \pm 0.3)$ MPa, and $E_5 = (2.2 \pm 0.4)$ MPa. As the surface was flattened totally, the additional sputtering of Au increased overall stiffness to $E_6 = (4.5 \pm 0.3)$ MPa.

1.3. Conservation of Compressive Stress within the Elastomeric Substrate — A Phenomenological Examination

Wrinkle patterns formed using the same plasma treatment parameters depend on the elastic modulus E_s of the PDMS film and evolve over time, as shown in Figure 3A. For a plasma-treated PDMS film with $E_s = 1$ MPa, wrinkles before Au deposition exhibited an amplitude of (90 ± 20) nm and a periodicity of (2.6 ± 0.2) μm . In Figure 3B, we show that compressive stress in the flattened electrode was maintained, as the subsequent peeling off of 30 nm sputtered Au electrode with adhesive tape returned the surface to a wrinkle pattern again. It showed a periodicity of (1.9 ± 0.1) μm and the amplitude of only (52 ± 5) nm. Compared to the wrinkling pattern before sputtering the Au electrode, the periodicity and amplitude are reduced by 27% and 42%, respectively. In addition, one observes a local alignment of wrinkles, cf. Figure 3B. We assume that an Au layer of a few nanometer remained on the PDMS, which was also visually observed when the sample was tilted against a light source, showing a golden shimmer. Figure 3C shows a closer look at the edge of Au/PDMS- O_x . In the region around the electrode, the wrinkles align parallel to each other and perpendicular to the electrode edge. They remain in this conformation along 100 μm , before returning to a randomly oriented arrangement. The amplitude of wrinkles rapidly increases in line with distance away from the electrode edge and reaches its equilibrium value within tens of micrometer, cf. Figure 3C. The periodicity of the oriented wrinkles was (2.4 ± 0.2) μm . The alignment of wrinkle patterns on the edges of PDMS surfaces has been reported by Bowden et al. as being due to stress relaxation at edges.^[32] The presence of nonoriented wrinkle patterns prior to the sputter deposition of Au indicates that a rearrangement of the wrinkles occurs during the sputtering process outside the deposition area. We assume that the heat load during sputtering caused the film to expand, and as the structure cooled down, it gave rise to wrinkles that were aligned with respect to the electrode edge.

An in situ study of the Au/MPTMS/SiO_x/PDMS heterostructure is presented in Figure 4. The extinction coefficient k and the real part ϵ' of the dielectric function are determined with respect to the Au film thickness in Figure 4B of the thermally evaporated Au on the multilayered PDMS/SiO_x/MPTMS nanostructure, as schematically illustrated in Figure 4A. These parameters of the dielectric function allow for the detailed investigation of Au film formation processes and for the quantification of the film morphology after deposition.^[39] The extinction coefficient reveals a broad plasmon absorbance band at a wavelength of 950 nm for Au film thicknesses below 3 nm. This is accompanied by a negative shift in the real part of the dielectric function, characteristic of confined electron oscillations on gold nanoparticles.^[40] However, at Au film thicknesses above 3 nm, this absorbance band vanishes while a sharp absorbance peak occurs at a wavelength around 600 nm. The increased mean path of electron oscillations for the first Au monolayers can be accounted by its enhanced adhesion to the MPTMS, thereby promoting confluent film growth. The sudden blue shift of the plasmon resonance indicates a pronounced Vollmer–Weber growth mode toward Au nanoparticles instead of confluent film formation for Au film thicknesses above 3 nm.^[39] With increased Au film thickness, this absorbance peak redshifts back toward the near infrared of the detected spectrum, thus indicating the coalescence of Au nanoparticles. The derived Au film thickness h_{Au} is higher compared to the expected film thickness, adjusted by the evaporator temperature. This fact underlines the Vollmer–Weber growth mode.^[40] The derived growth rate h_{Au}' in Figure 4E asymptotically approaches the adjusted growth rate d' , exhibiting an insulator–metal transition (IMT) above a derived Au thickness of (14 ± 2) nm.^[39] The IMT threshold coincides with a rapid redshift of the absorbance feature within extinction coefficient spectra for film Au thicknesses above 12 nm, indicating the onset of free electron oscillations. Thus, this detected percolation threshold for Au growth on MPTMS/SiO_x/PDMS is well below that of Au growth on untreated PDMS at 22 nm.^[39] This is in accordance with the improved conductivity of Au electrodes on MPTMS/SiO_x/PDMS compared to Au electrodes on untreated PDMS, verified by a four-point probe measurement.^[20] The sharp absorbance feature around a wavelength of 400 nm is related to scattering on the surface's wrinkled microstructure. The negligible shift of this absorbance indicates stable wrinkled morphology during Au deposition.

1.4. Long-Term Stability of Compressed Au Electrodes

In Figure 5, we compare AFM topography scans of a sputtered 30 nm thin Au electrode on the native PDMS and on the MPTMS/SiO_x/PDMS surfaces. The calculated root-mean-square roughness value for a 2×2 μm^2 area was found to be (1.5 ± 0.2) nm for the sputtered 30 nm Au electrode on native PDMS, whereas the same Au electrode on MPTMS/SiO_x/PDMS showed a value of (0.5 ± 0.1) nm. Long-term observations show that the poor adhesion of the initially flat Au electrode on native PDMS leads to the formation of Au nano-clusters with dome-like structures having an average diameter of 100 nm and a height up to 50 nm. In addition, DEAs with

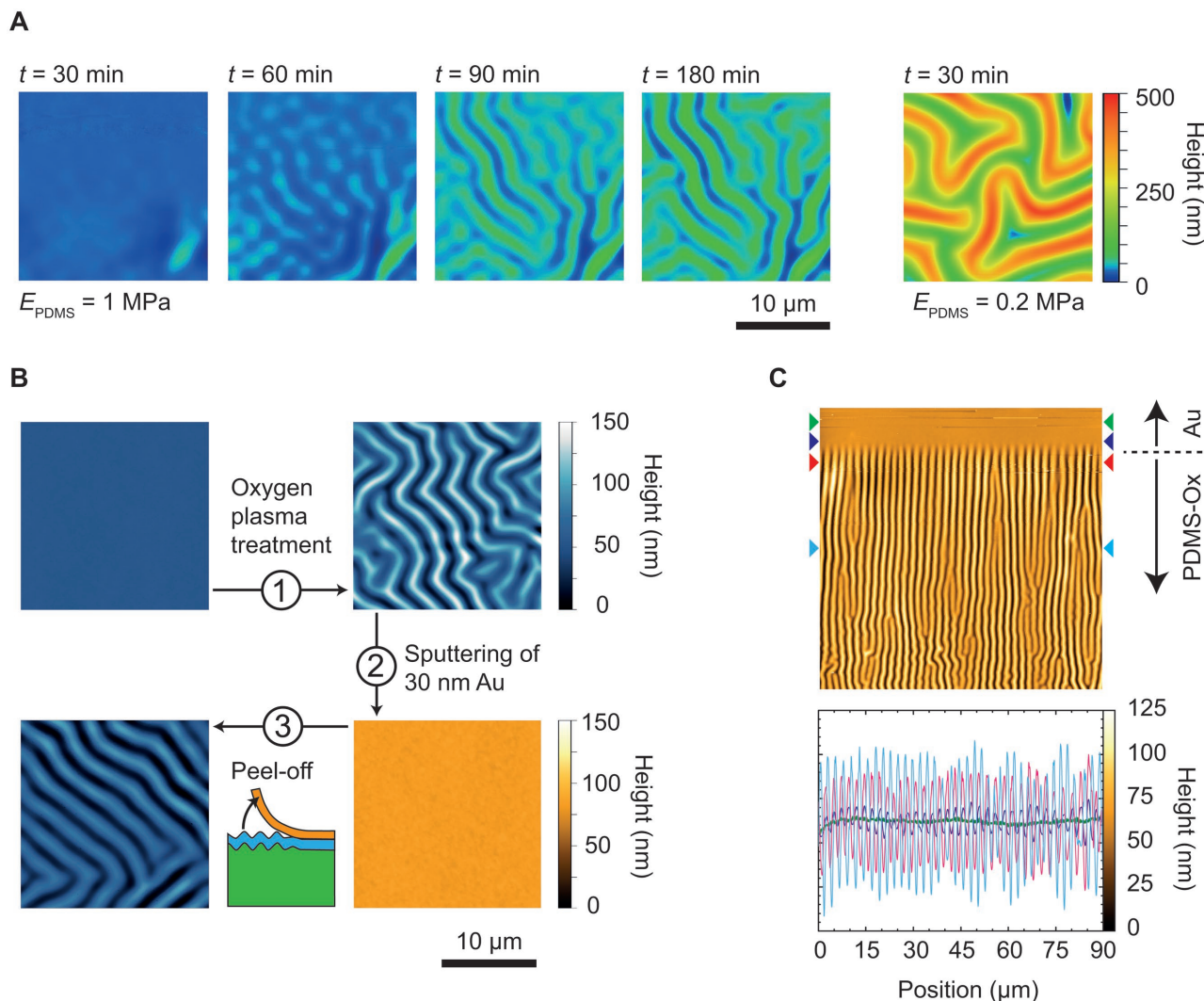


Figure 3. Relaxation of a compressed Au electrode on an elastomeric substrate to a wrinkled pattern after peeling off the Au electrode. A) Reformation of the PDMS surface, with $E_{S1} = (1.0 \pm 0.1)$ MPa and $E_{S2} = (0.2 \pm 0.1)$ MPa after oxygen-plasma treatment. Reformation is finished much faster for the softer PDMS with E_{S2} . B) The prestressed structure with a 30 nm Au on top of a wrinkled surface went back to a wrinkled structure again after peeling off the thin Au layer. C) An AFM scan at step Au/PDMS- O_x electrode. The wrinkles were aligned parallel to each other and perpendicular to the Au electrode edge. This conformation is found for a region of about 100 μm . Profile cuts with locations indicated by the colored arrowheads show that the wrinkle amplitude rapidly increases in line with distance to the electrode edge, which implies that the wrinkles are flattened and not filled with Au, due to material transport phenomena. Insulator-to-metal transition of Au on a compressed and MPTMS-functionalized PDMS- O_x surface.

compressed Au electrodes were still ready for operation after a period of nine months.

1.5. Fabrication and Actuation of DEAs with Compressed Au Electrodes

Substrate-based thin-film DEAs, using MPTMS as an interface between PDMS- O_x and an Au electrode, were fabricated as shown in **Figure 6A**. The actuation of the DEA was measured by detecting the curvature k_s of the underlying PEN cantilever as a function of the applied voltage U , using an optical beam deflection technique, cf. **Figure 6B**. This technique permits the measurement of actuation forces in dielectric elastomeric transducers with elastomer layers as thin as 1 μm .^[35]

The asymmetric cantilevers consisted of 8 μm thin DEAs (15 nm Au/8 μm PDMS/15 nm Au) deposited on 50 μm thick PEN substrates. The application of a voltage generated electrostatic pressure that was translated to an in-plane expansion of the DEA. The torque of this asymmetric actuation bent the PEN cantilever. The real-time response of the curvature k_s in **Figure 6C** corresponded well to the predicted model with the square dependence to the applied voltage U

$$k_s = \frac{1}{R} = U^2 \frac{6\epsilon_0\epsilon_p(1-\nu_s)(h_p+h_s)}{E_s h_p h_s^3} \quad (4)$$

where thickness h_p and permittivity ϵ_p are parameters of the PDMS membrane, and thickness h_s , the elastic modulus E_s , and Poisson's ratio ν_s are parameters of the PEN substrate. The

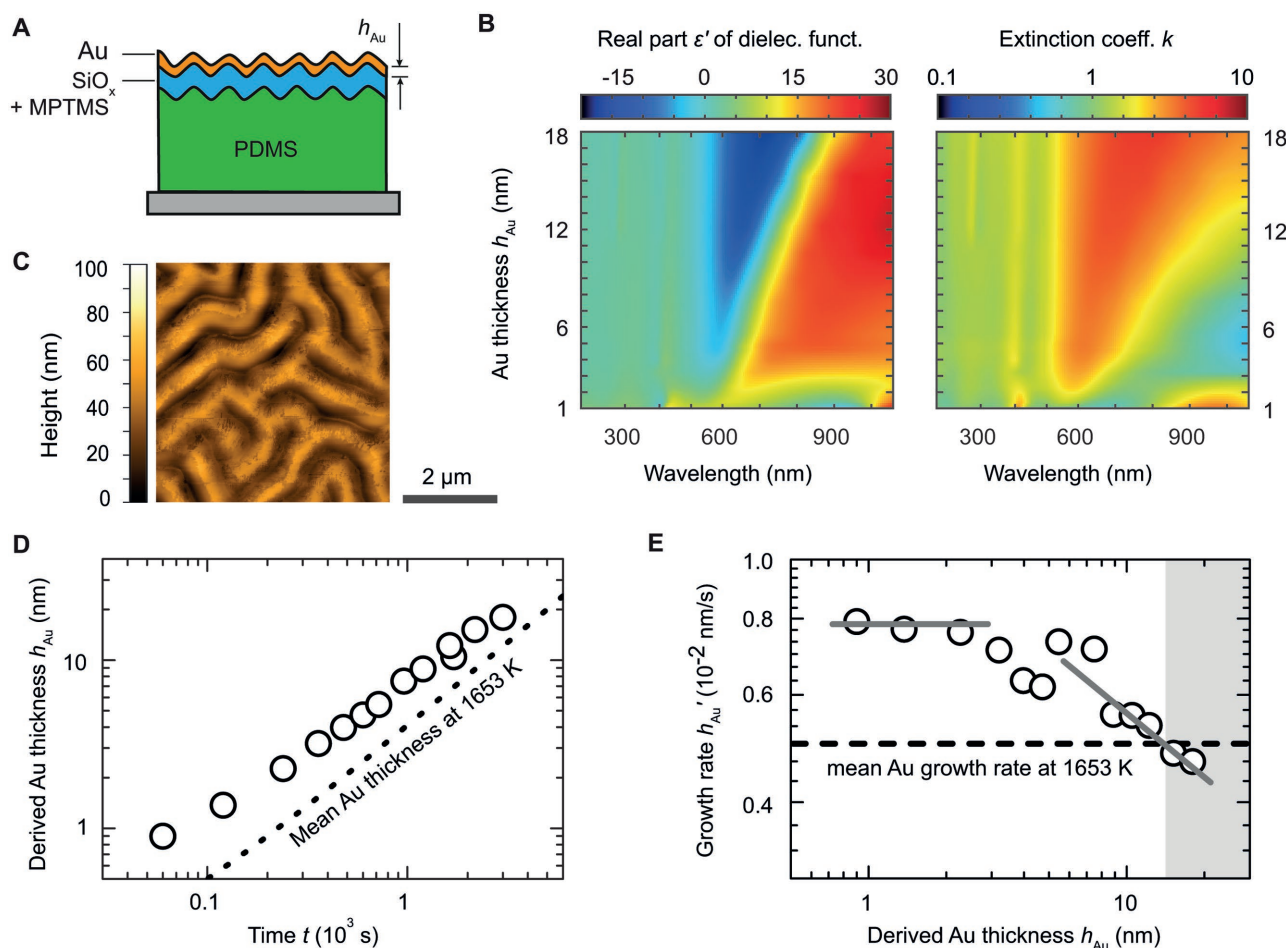


Figure 4. Insulator-to-metal transition for thermally evaporated Au on MPTMS/SiO_x. A) Schematic description of the stacked nanostructures. B) The evolution of the extinction coefficient k and the real part ϵ' of the dielectric function with respect to Au film thickness on a wrinkled MPTMS/SiO_x/PDMS surface. The color code for the extinction coefficient k and the real part ϵ' of the dielectric function is displayed logarithmically and linearly, respectively. C) AFM scan of the evaporated Au electrode. D) The ellipsometry-derived Au film thickness h_{Au} at representative time points for Au growth on the wrinkled MPTMS/SiO_x/PDMS surface. The dotted line represents the mean Au thickness adjusted by the evaporator temperature at 1653 K. E) Ellipsometry-derived growth rates h'_{Au} of Au with respect to the derived Au thickness h_{Au} . The expected mean growth rate for an evaporation temperature of $T = 1653$ K is marked as a dashed line.

applied electrical field perpendicular to the PDMS layer was $120 \text{ V } \mu\text{m}^{-1}$ with leakage currents below the detection limit of $10 \text{ } \mu\text{A}$. This value is 50% higher than in previous reports for the same PDMS.^[35,41] The results are consistent with recently performed simulations, which show that the surface tension increase leads to a significant improvement of the critical electrical field for instabilities to occur in constrained dielectric elastomer films.^[42]

2. Conclusions

We have demonstrated an innovative approach to realize soft Au electrodes on silicone substrates. Our results, combining topological and mechanical film properties, shed light on the formation and reformation of wrinkles associated with the intrinsic compression of metal films. More generally, the interplay between a metal electrode and an elastomer substrate allows for tuning local morphology and related mechanics.

Especially important is the ability to suppress the stiffness impact of the thin metal electrode on the entire sandwich nanostructure. Once the electrode has a thickness at which wrinkles disappear, maximal compliance is reached. Ultrathin-film dielectric elastomer transducers, which can be operated at low voltages, require such intrinsic-compressed, soft electrodes. Especially for dielectric elastomer actuators with thousands of nanometer-thin layers, this approach to suppress any rise in stiffness is productive.

3. Experimental Section

Preparation of the DEA Structures: PDMS (Dow Corning 184 Silicone Elastomer Kit, Dow Corning Europe S.A, Belgium) was prepared by mixing the prepolymer (component A) and the crosslinker (component B) at a volume ratio of 10:1, degassing for a period of 30 min, and then spin-coating on a 2 in. Si wafer at a rotation speed of 6000 rpm for a period of 120 s. The PDMS films were thermally cured at a temperature of $75 \text{ } ^\circ\text{C}$ for a period of 24 h. For the in situ ellipsometry measurements

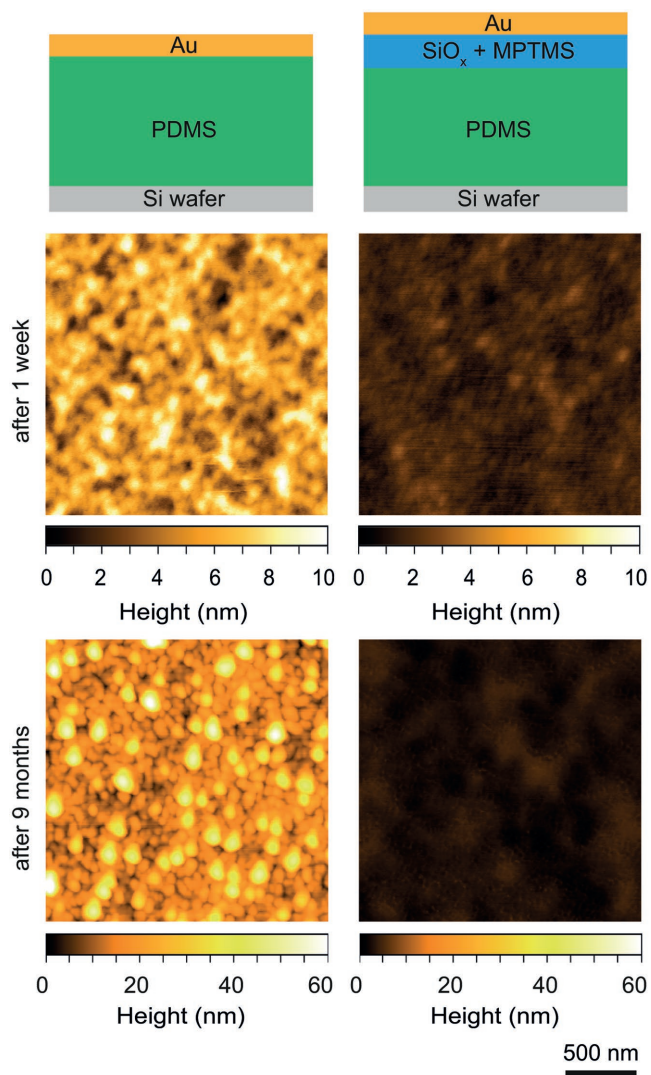


Figure 5. ULong-term stability of compressed Au electrodes. AFM scans of 30 nm thin sputtered Au electrodes. The Au electrode on native PDMS shows the characteristic morphology related to Au clusters, whereas the compressed Au electrode is flat with a roughness of 0.5 nm. The formation of Au nanoclusters on PDMS after nine months' storage in air at room temperature is suppressed for the compressed Au electrode.

in Figure 4, vinyl-terminated PDMS DMS-V05 (Gelest Inc., Morrisville, PA, USA) was evaporated at a temperature of (160 ± 5) °C and deposited on a 2 in. Si wafer inside a UHV chamber at a base pressure of 10^{-7} mbar, using low-temperature effusion sources (NTEZ, Dr. Eberl MBE Komponenten GmbH, Weil der Stadt, Germany) with a 25 cm³ crucible. Crucible temperature was well below the temperature required to thermally degrade vinyl end groups.^[43] The Si wafer was mounted at a distance of 400 mm away from the crucibles. The plasma treatments were performed on a 40 kHz RF system (PICO System, Diener Electronics, Ebhausen, Germany). The chamber was floated with oxygen at a flow rate of 20 sccm (Carbagas AG, Gümligen, Switzerland), keeping the partial pressure constant at 0.3 mbar. MPTMS of a purity $\geq 94.5\%$ (Sigma-Aldrich, Switzerland, CAS Number: 4420-74-0, formula: C₆H₁₆O₃SSi, formula weight: 196.34 g mol⁻¹) was deposited on the hydroxyl PDMS surface by floating the vacuum chamber at 0.1 mbar for a period of 60 min. Excess MPTMS was removed by putting the sample in an ethyl acetate bath (Merck KGaA, Darmstadt, Germany). The Au electrodes (Lesker, East Sussex, UK) were sputtered using a DC sputter

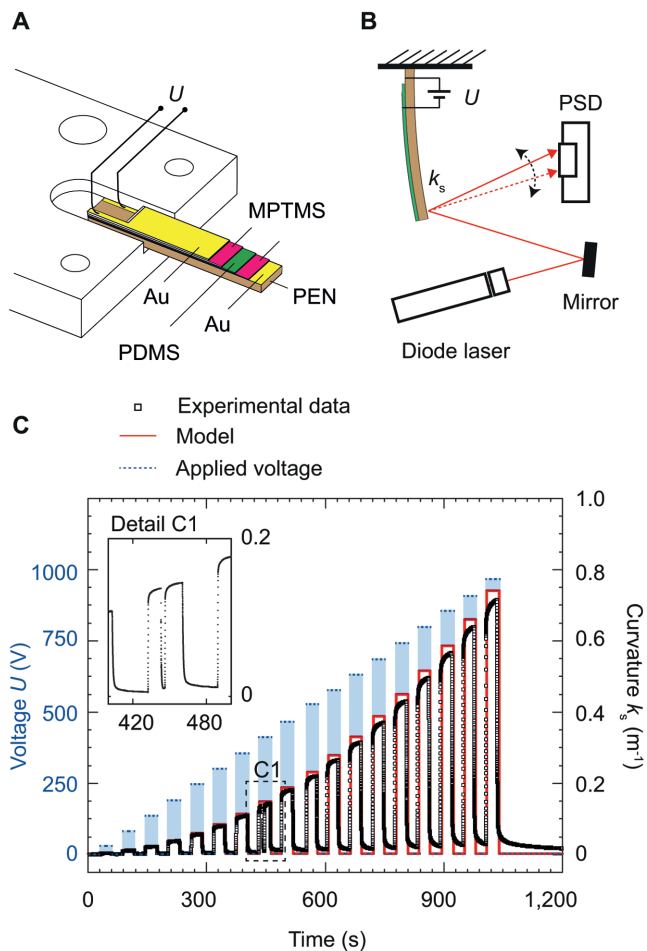


Figure 6. Actuation characteristics of bending DEA cantilever structures with compressed electrodes. A) Preparation of the DEA/PEN cantilever with a free-hanging area of 4×12 mm². B) Schematic illustration of the optical beam deflection method. For small deflections, curvature k_s can be calculated from the displacement of the laser beam on the PSD. C) Real-time response of the actuation up to an applied electrical field of $120 \text{ V } \mu\text{m}^{-1}$. The model originates from Equation (4). Detail C1 shows a selfclearance effect occurring at $53 \text{ V } \mu\text{m}^{-1}$, where the DEA structure recovered after a short breakdown due to defects in the dielectric layer.

coater (SCD040, Balzers Union, Liechtenstein) at a discharge current of 15 mA. The sputter chamber was floated with Ar, and the pressure was kept at 0.05 mbar (Carbagas AG, Gümligen, Switzerland). The thickness of the Au electrodes was monitored using a quartz crystal microbalance (QSG 301, Balzers Union, Liechtenstein). The actuation measurements of DEAs were performed using a high-voltage supply (Stanford Research System PS310, GMP SA, Lausanne, Switzerland) with a current resolution of 10 μA .

AFM Imaging and Nanoindentation: AFM images were acquired by raster scanning the region of interest with a soft AFM probe (Tap190Al-G probe, NanoAndMore GmbH, Wetzlar, Germany) in tapping mode (FlexAFM C3000, Nanosurf AG, Liestal, Switzerland). The raw data were leveled by subtracting a mean plane and a polynomial background of second degree. Root-mean-square roughness values were calculated using the open source software for SPM data analysis, Gwyddion, Version 2.41. AFM nanoindentation measurements using a spherical tip with a radius of (522 ± 4) nm (B500FMR, Nanotools GmbH, Germany) were carried out to assess the mechanical properties of the soft heterostructures. Areas of $10 \times 10 \mu\text{m}^2$ were partitioned into 2500 domains, each serving as a nanoindentation site. The elastic modulus

at each site was calculated from the related force–distance curve by means of the Hertz contact model, as implemented in the FLEX-ANA software (Automated Nanomechanical Analysis, Nanosurf AG, Liestal, Switzerland). Substrate effects could be ignored, since the indentation depths were well below 500 nm.

Real-Time Spectroscopic Ellipsometry: To extract the optical properties of the nanostructures formation in situ, a spectroscopic ellipsometer (SE801, Sentech, Berlin, Germany) with SpectraRay3 software was utilized. The ellipsometric Ψ and Δ values from light with wavelengths ranging from 190 to 1050 nm were monitored at a frequency of 0.5 Hz at an incident angle of 70° to the normal of the substrate's surface. The 4 mm diameter of the incident beam led to a $4 \times 10 \text{ mm}^2$ spot area on the substrate. The obtained Ψ and Δ values were related to the complex Fresnel reflection coefficients r_p and r_s of p- and s-polarized light and their ratio ρ by

$$\rho = \frac{r_p}{r_s} = e^{-i\Delta} \tan \Psi \quad (5)$$

Based on the obtained Fresnel reflection coefficient ratio, it was possible to extract the wavelength-dependent dielectric function $\varepsilon(\lambda)$

$$\begin{aligned} \langle \varepsilon \rangle &= \langle \varepsilon' \rangle + i \langle \varepsilon'' \rangle = \langle \tilde{n} \rangle^2 = [\langle n \rangle + i \langle k \rangle]^2 \\ &= \varepsilon_0 \sin^2(\varphi_0) \left[1 + \tan^2(\varphi_0) \left(\frac{1-\rho}{1+\rho} \right)^2 \right] \end{aligned} \quad (6)$$

with an angle of incidence φ_0 , vacuum permittivity $\varepsilon_0 = 1$, and $n(\lambda)$ the real and $k(\lambda)$ the imaginary parts of the refractive index, respectively. The dielectric function of the evaporated PDMS was modeled with the Tauc–Lorentz dispersion formula.^[44] To model the dielectric function of Au, a combination of two dispersion types was applied, named the “Drude–Lorentz oscillator model”. Here, the Drude oscillator described the absorption of free-charge carriers, assuming that they acted in phase in response to the applied electrical field, while the Lorentz oscillator effectively modeled electrons bound to a positive core.^[45] For the assessment of the model, the mean square error of the model fit and the experimentally measured $\Psi^{\text{mod,exp}}$ and $\Delta^{\text{mod,exp}}$ were calculated as

$$\text{MSE} = \frac{1}{N} \sqrt{\sum_{i=1}^N \left[\left(\frac{\Psi_i^{\text{mod}} - \Psi_i^{\text{exp}}}{\sigma_{\Psi_i}^{\text{exp}}} \right)^2 + \left(\frac{\Delta_i^{\text{mod}} - \Delta_i^{\text{exp}}}{\sigma_{\Delta_i}^{\text{exp}}} \right)^2 \right]} \quad (7)$$

with the random and systematic error σ^{exp} .

Supporting Information

Supporting Information is available from the Wiley Online Library or from the authors.

Acknowledgements

The authors acknowledge the financial support of the nano-tera.ch initiative, project SmartSphincter, as well as the Swiss Nanoscience Institute (SNI) for the financial contribution to the AFM. The authors thank Nanotools GmbH, Germany, for kindly providing them with two extra B500 AFM cantilevers, Frederikke Bahrt Madsen at the Technical University of Denmark, Florian M. Weiss and Vanessa Leung at the University of Basel for their helpful discussions and feedback on the paper.

Conflict of Interest

The authors declare no conflict of interest.

Keywords

AFM nanoindentations, dielectric elastomer transducers, metal-on-elastomer films, oxygen-plasma treatment of PDMS, soft electrodes

Received: April 27, 2017

Revised: June 6, 2017

Published online:

- [1] R. Pelrine, R. Kornbluh, Q. Pei, J. Joseph, *Science* **2000**, *287*, 836.
- [2] Y. Bar-Cohen, *Electroactive Polymer (EAP) Actuators as Artificial Muscles: Reality, Potential, and Challenges*, SPIE Press, Bellingham, **2004**.
- [3] P. Brochu, Q. Pei, *Macromol. Rapid Commun.* **2010**, *31*, 10.
- [4] I. A. Anderson, T. A. Gisby, T. G. McKay, B. M. O'Brien, E. P. Calius, *J. Appl. Phys.* **2012**, *112*, 041101.
- [5] G. Rizzello, D. Naso, A. York, S. Seelecke, *Smart Mater. Struct.* **2016**, *25*, 035034.
- [6] F. Carpi, D. De Rossi, R. Kornbluh, R. E. Pelrine, P. Sommer-Larsen, *Dielectric Elastomers as Electromechanical Transducers: Fundamentals, Materials, Devices, Models and Applications of an Emerging Electroactive Polymer Technology*, Elsevier, Amsterdam, **2008**.
- [7] D. Rus, M. T. Tolley, *Nature* **2015**, *521*, 467.
- [8] E. Fattorini, T. Brusa, C. Gingert, S. Hieber, V. Leung, B. Osmani, M. D. Dominiotto, P. Büchler, F. Hetzer, B. Müller, *Ann. Biomed. Eng.* **2016**, *44*, 1355.
- [9] A. Poulin, S. Rosset, H. R. Shea, *Appl. Phys. Lett.* **2015**, *107*, 244104.
- [10] T. Töpfer, F. M. Weiss, B. Osmani, C. Bippes, V. Leung, B. Müller, *Sens. Actuators, A* **2015**, *233*, 32.
- [11] F. M. Weiss, T. Töpfer, B. Osmani, S. Peters, G. Kovacs, B. Müller, *Adv. Electron. Mater.* **2016**, *2*, 1500476.
- [12] R. Pelrine, R. Kornbluh, J. Joseph, R. Heydt, Q. Pei, S. Chiba, *Mater. Sci. Eng., C* **2000**, *11*, 89.
- [13] F. B. Madsen, A. E. Daugaard, S. Hvilsted, A. L. Skov, *Macromol. Rapid Commun.* **2016**, *37*, 378.
- [14] I. M. Graz, D. P. J. Cotton, S. P. Lacour, *Appl. Phys. Lett.* **2009**, *94*, 071902.
- [15] S. Rosset, H. R. Shea, *Appl. Phys. A* **2013**, *110*, 281.
- [16] R. Seghir, S. Arscott, *Sci. Rep.* **2015**, *5*, 14787.
- [17] J. Tang, H. Guo, M. Zhao, J. Yang, D. Tsoukalas, B. Zhang, J. Liu, C. Xue, W. Zhang, *Sci. Rep.* **2015**, *5*, 16527.
- [18] D. McCoul, W. Hu, M. Gao, V. Mehta, Q. Pei, *Adv. Electron. Mater.* **2016**, *2*, 1500407.
- [19] A. Hirsch, H. O. Michaud, A. P. Gerratt, S. Mulatier, S. P. Lacour, *Adv. Mater.* **2016**, *28*, 4507.
- [20] B. Osmani, H. Deyhle, F. M. Weiss, T. Töpfer, M. Karapetkova, V. Leung, B. Müller, *Proc. SPIE* **2016**, *9798*, 979822.
- [21] Y.-L. Loo, R. L. Willett, K. W. Baldwin, J. A. Rogers, *Appl. Phys. Lett.* **2002**, *81*, 562.
- [22] T. Adrega, S. P. Lacour, *J. Micromech. Microeng.* **2010**, *20*, 055025.
- [23] B. Atmaja, J. Frommer, J. C. Scott, *Langmuir* **2006**, *22*, 4734.
- [24] A. K. Mahapatro, A. Scott, A. Manning, D. B. Janes, *Appl. Phys. Lett.* **2006**, *88*, 151917.
- [25] H. Hillborg, J. F. Ankner, U. W. Gedde, G. D. Smith, H. K. Yasuda, K. Wikström, *Polymer* **2000**, *41*, 6851.
- [26] K. Efimenko, W. E. Wallace, J. Genzer, *J. Colloid Interface Sci.* **2002**, *254*, 306.
- [27] D. Bodas, C. Khan-Malek, *Sens. Actuators, B* **2007**, *123*, 368.
- [28] D. B. H. Chua, H. T. Ng, S. F. Y. Li, *Appl. Phys. Lett.* **2000**, *76*, 721.
- [29] D. Y. Khang, J. A. Rogers, H. H. Lee, *Adv. Funct. Mater.* **2009**, *19*, 1526.
- [30] A. Schweikart, A. Fery, *Microchim. Acta* **2009**, *165*, 249.

- [31] N. Bowden, S. Brittain, A. G. Evans, J. W. Hutchinson, G. M. Whitesides, *Nature* **1998**, 393, 146.
- [32] N. Bowden, W. T. S. Huck, K. E. Paul, G. M. Whitesides, *Appl. Phys. Lett.* **1999**, 75, 2557.
- [33] Y. Shao, M. A. Brook, *J. Mater. Chem.* **2010**, 20, 8548.
- [34] T. R. Hendricks, I. Lee, *Nano Lett.* **2007**, 7, 372.
- [35] B. Osmani, E. A. Aeby, B. Müller, *Rev. Sci. Instrum.* **2016**, 87, 053901.
- [36] W. T. S. Huck, N. Bowden, P. Onck, T. Pardoen, J. W. Hutchinson, G. M. Whitesides, *Langmuir* **2000**, 16, 3497.
- [37] S. Béfahy, P. Lipnik, T. Pardoen, C. Nascimento, B. Patris, P. Bertrand, S. Yunus, *Langmuir* **2010**, 26, 3372.
- [38] B. Osmani, G. Gerganova, B. Müller, *Eur. J. Nanomed.* **2017**, 9, 69.
- [39] T. Töpfer, S. Lörcher, B. Osmani, V. Leung, H. Deyhle, T. Pfohl, B. Müller, *Adv. Electron. Mater.* **2017**, 1700073.
- [40] T. W. H. Oates, L. Ryves, M. M. M. Bilek, *Opt. Express* **2008**, 16, 2302.
- [41] D. Gatti, H. Haus, M. Matysek, B. Frohnapfel, C. Tropea, H. F. Schlaak, *Appl. Phys. Lett.* **2014**, 104, 052905.
- [42] S. Seifi, H. S. Park, *Int. J. Solids Struct.* **2016**, 87, 236.
- [43] T. Töpfer, S. Lörcher, F. M. Weiss, B. Müller, *APL Mater.* **2016**, 4, 056101.
- [44] H. Fujiwara, *Spectroscopic Ellipsometry: Principles and Applications*, John Wiley & Sons, Hoboken, NJ, USA, **2007**.
- [45] T. W. H. Oates, H. Wormeester, H. Arwin, *Prog. Surf. Sci.* **2011**, 86, 328.